SYMMETRY AND NON-LINEARITY IN FINITE ELEMENT FRACTURE ANALYSIS*

P.S. CHOPRA, B. MOUSTAKAKIS and T.S. WU

EBR-2 Project, Argonne National Laboratory, Argonne, Illinois 60439, U.S.A.

SUMMARY

The formation of symmetrical and non-symmetrical branch and secondary cracks is investigated using the finite element method and a total energy rate technique for fracture analysis. The study focuses on the influence of fracture morphology and changing boundary conditions on the construction of analytical models for fracture investigations.

Conditions of loading, material and geometric symmetry in a structure are necessary but not sufficient for the use of symmetry in constructing the analytical model for fracture where it is necessary that the fracture profiles to be investigated also be symmetric in the same sense as are the loading, material and geometry. Part-through radial cracks in an axisymmetric shell are investigated for the violation of symmetry with respect to a segment of the shell due to large local and global deformations. In addition, the influence of changes in force boundary conditions on the deformation of the shell is investigated as a function of fracture propagation.

The study demonstrates that the more probable fracture configurations are non-symmetrical and in some cases, initially symmetrical configurations may propagate to a non-symmetrical configuration. In such cases it is desirable to use a non-segmented analytical model, without regard to symmetry, to investigate the initial symmetrical configurations as well as the subsequent non-symmetrical configurations. This will minimize computational differences due to finite element mesh changes.

* This work has been performed under the auspices of the United States Atomic Energy Commission.

1. Introduction

Any fracture investigation of polycrystalline materials must consider non-homogeneities in the form of inclusions and flawed boundaries, which have lower resistance to fracture than the surrounding material. In reality, the Griffith model of a perfectly smooth crack [1]* contradicts the observed multiple and irregular fractures exhibited in service failures as shown in Figs. 1 and 2.

In an earlier work [2,3] the finite element method was used to investigate symmetric and non-symmetric fracture configurations. Using the total strain energy rate approach, and the finite element results for an edge-cracked panel it was demonstrated that non-symmetric fracture configurations have a higher probability of formation and propagation, than do symmetric configurations.

In this presentation, the total strain energy release rate approach is used to investigate the effects of lack of symmetry and linearity on the fracture propagation configurations. Lack of symmetry and linearity may be caused by large global and local deformations, multiple secondary cracks or additional constraints on the displacement of the structure.

The fracture of an edge-cracked panel and a cylindrical shell element are considered. For the edge-cracked panel, an attempt is made to determine the effect of the deformation of the panel under a uniaxial tensile stress on the fracture propagation pattern. In a separate case, an additional restriction on the panel displacements is imposed in the form of roller support of the uncracked free edge of the panel. For the cylindrical shell element, the effect on the fracture propagation of large deformations which destroy the symmetry of the cross section is examined. The effects of pressure loading on the crack surface and of local loads adjacent to it also are investigated.

2. Analysis Approach

The general instantaneous energy criterion for fracture is written in terms of the Hartz function, H, as [2]:

$$H(a_T) = \frac{\Delta U(a_T)}{-\Delta a_T} - \frac{\Delta S(a_T)}{\Delta a_T} \geq 0, \tag{1}$$

or, equivalently,

$$H(a_T) = G(a_T) - R(a_T) \geq 0. \tag{2}$$

Here, a_T is the fracture area, $U(a_T)$ is the total strain energy stored in the body, $G(a_T)$ is the instantaneous total strain energy release rate for crack formation, $R(a_T)$ is the instantaneous rate of conversion of available energy into the energy required for crack formation, and Δ is used to indicate the increment of a quantity.

The strain energy release rates $G_T(a_T)$ are obtained from finite element solutions of successive boundary value problems, corresponding to progressive fracture configurations. When the total strain energy stored in the body is computed, the strain energy release rate is written as:

---

*Numbers in brackets correspond to items under the references.

$$G_T(a_T) = \pm \frac{\Delta U(a_T)}{\Delta a_T} , \qquad (3)$$

where the plus sign applies in the case of constant stress boundary conditions and the minus sign in the case of fixed displacement boundary conditions.

It has been hypothesized [2] that *in an elastic solid body experiencing fracture under the action of specified surface tractions, the relative locations, size and orientation of crack initiation and propagation configurations are determined by the corresponding values of the Hartz function H.*

Figure 3 shows the edge-cracked panel, which is three inches long and one inch wide, under uniaxial tensile stress of 1000 psi. The cylindrical shell segment analyzed is shown in Fig. 4, with an inner radius of one inch and thickness equal to 0.012 inches under uniform internal pressure of 1000 psi. Both were assumed to be perfectly homogeneous and isotropic. The panel was of Holomite 100 material with Young's modulus of 500,000 psi and Poisson's ratio of 0.35. The shell was assumed to be of type 304 stainless steel with Young's modulus equal to 23,500,000 psi and Poisson's ratio equal to 0.30.

The material parameter, R_T, was assumed to be constant. It was sufficient, therefore, to investigate the total instantaneous strain energy release rate, G_T.

The finite element code derived by Wilson [4], using the constant strain triangular element [5] was employed with a slight modification to compute the strain energy stored in each element and its summation over the entire body.

3. Results and Discussion

Results were obtained for various fracture configurations of the rectangular panel under uniaxial stress and the cylindrical shell under internal pressure. The finite element mesh representations used for the two cases are shown in Figs. 3 and 4.

The results of simulation of a single smooth crack of gradually increasing length are shown in Fig. 5, where the total instantaneous strain energy release rate, G_T, is plotted as a function of the crack length, a_T. As expected, the shape of the curve suggests that crack propagation becomes easier with increasing length of crack, as indicated by the higher values of G_T.

The effects of large deformations and changing boundary conditions are considered next. Four different cases are selected to include the effects of non-linearity and changing boundary conditions. A free-body diagram of the plate in each of these four cases is shown in Fig. 6. In Fig. 6(a) the free-body diagram of a rectangular panel under uniaxial tension, but not otherwise constrained, is shown. With the crack as shown in the figure, deformation of the panel will follow the pattern shown by the dashed lines; the applied stress, perpendicular to the right edge of the plate, will induce bending stresses and a vertical reaction will be needed on the left edge of the plate in order to maintain static equilibrium, thus changing the boundary conditions initially postulated for that edge.

In order to account for these changes the deformed configuration of the finite element grid was used as input in subsequent simulations. A graphical illustration of the procedure is given in Fig. 7. A structure of stiffness k_{11} is loaded with a load P, causing a deflection OE. As the crack propagates, the stiffness of the structure is reduced to k_{12}, and the deflection is increased by the amount EF. The strain energy stored in the structure

changes from U_{11} to U_{12} as shown by the areas under the P-δ curves. A multiple of the strain energy release rate, G_1 is shown by the shaded area in the figure. The deformed structure has a different stiffness k_{21} at the initial stage and k_{22} at the final stage of the fracture configuration and the amount of strain energy stored changes from U_{21} to U_{22} during the crack propagation, giving a strain energy release rate, G_2.

The objective of this study was to examine the relative changes in U and G when the structure is deformed from its unloaded state, causing a change in its effective stiffness.

The misalignment of the plate, shown in the deformed case of Fig. 6(a) may be prevented by placing additional constraints on the displacements of the bottom edge of the plate, in the form of roller support. A free-body diagram for that case is shown in Fig. 6(b). The deformed panel is shown with dashed lines, but this time no changes occur in boundary conditions or bending stresses.

Results obtained by finite element simulation of a non-symmetric fracture configuration, in all four cases, are shown in Fig. 8, where the strain energy release rate, G_T, is plotted as a function of the angle of crack propagation. These results, of course, verify earlier conclusions regarding the slope of the strain energy release rate curve, and the most probable path of crack propagation. For the cases studied the results predict non-symmetrical zig-zag propagation, as shown in Fig. 2.

In addition, the non-linear effect of the *elastic deformation* is in each case negligible. The same is not true of the effect of *boundary conditions* obtained by restricting the plate to uniaxial deformation. The addition of rollers on the free side of the panel reduces the total strain energy release rate significantly. This is because the roller supports restrict the non-linear changes in boundary conditions described in Fig. 6(a). Thus, with constrained boundaries, the probability of crack formation and propagation is reduced.

In addition to the total strain energy release rate, G_T, the total strain energy U_T stored in the panel was greater in the case of the free edge than in the case of the roller-supported edge, and increased with increasing deformation, as shown in Table I.

The results presented in Fig. 8 and Table I were examined further with the help of two additional fracture mechanics parameters: the crack opening displacement, COD, and the stress intensity factor, K_1 [6]. The COD was expressed in terms of the displacement of a nodal point on the crack surface orthogonal to the crack propagation direction. A positive value was assigned to a COD which separated the crack surfaces. The stress intensity factor was expressed in terms of the crack opening stress, COS, which is the component of the stress tensor orthogonal to the crack propagation direction, in an element immediately ahead of the crack tip. The limitations of the use of stress intensity factors and crack opening displacements in multiple fracture analyses have been discussed [2]. However, an examination of these parameters, specifically defined as above, is useful for purposes of comparison with energy release rate predictions.

Figure 9 shows the values of the crack opening displacements and the crack opening stresses for cases A, B, C and D as defined in Fig. 8. The results demonstrate the total consistency between the relative values of COD with the results obtained for U_T and G_T. The crack opening stresses also are reduced by the addition of rollers. However, the crack opening stresses are lower for the deformed geometries in contradiction to the results

obtained for U_T, G_T and COD. These inconsistencies, however small, are attributed to the ambiguity present in selecting the element ahead of the crack tip and the stress component for computing COS [2]. Thus predictions made on the basis of COS are questionable, particularly when the differences are as small as shown in Fig. 9.

Results for the cylindrical shell element were obtained for a smooth longitudinal crack on the inner surface of the shell, using both the initial and deformed geometries of the finite element grid. The crack was assumed to be long in comparison to the shell diameter so that plane strain analysis was justified.

Figure 10 shows the total strain energy release rate, G_T, as a function of the relative crack depth a_T/h for three cases. In case 1 the shell is loaded with internal fluid pressure of 1000 psi only. In case 2 one additional local load of 4000 lbs is applied in the vicinity of the crack. In case 3 the shell is under internal fluid pressure of 1000 psi and a local load of 4000 lbs applied 15° away from the crack. The loading described in case 2 resulted in a slight decrease of the total strain energy release rate. Case 3 loading increased that quantity appreciably.

Figure 11 shows the crack opening displacements and crack opening stresses for the three cases of loading described previously. Both COD and COS decrease in case 2 and increase in case 3. This is consistent with the findings in terms of G_T and U_T, suggesting that the relative locations of cracks and local loads are important in predicting fracture propagation properties.

As in the case of the rectangular panel, deformation of the shell changes both the total strain energy stored in the structure and the total strain energy release rate. When small elastic deformations are allowed, without appreciable change in the constraints of the structure, the change in the total strain energy release rate is not significant. Thus to obtain a measurable effect of the shell deformation on the fracture configuration, the internal fluid pressure was increased to 25,000 psi and a crack propagating from 5/8 to 3/4 of the shell thickness was investigated. Figure 12 shows the total strain energy release rates in both deformed and undeformed cases. Unlike the case of the rectangular panel, accounting for the deformation of the shell resulted in a decrease of the total strain energy release rate. This result appears inconsistent with those for the rectangular plate. However, this result may be explained by comparing the crack opening displacements and crack opening stresses for the shell.

Figure 13 shows the quantities of COD and COS for the cases of the deformed and undeformed geometries of the shell. With the deformed geometry a decrease occurs in both COS and COD, compared to results obtained with undeformed geometry. Hence the effect of the deformation is to close the crack and decrease both U_T and G_T.

Another non-linear effect is the increase of the percentage of area under load due to fluid pressure as the crack propagates. Under fluid pressure, the surface of the crack will also be loaded by the fluid, whereas under mechanical loading the surface of the crack will not be loaded. This effect has been investigated previously [7], and it was shown that the total strain energy release rate is higher in the case of fluid pressure. This result is shown in Fig. 14.

4. Conclusions

The results presented verify earlier predictions that non-symmetrical fracture configu-

rations have a higher probability of occurrence than do symmetrical configurations. This conclusion also applies when the deformation of a structure is considered or the boundary conditions are modified.

The strain energy stored in a structure, the strain energy release rate for crack propagation and the crack opening displacement were found to be consistent over a range of deformed and undeformed geometries of a plate and a shell element. Non-linear effects produced by elastic deformation were found to cause negligible changes in strain energy release rates. However, non-linearity due to large displacements, resulting in a change in the boundary conditions of the structure, produced significant changes in the strain energy release rates. Similar significant effects were observed when changes in pressure boundary conditions due to crack propagation were considered.

The study demonstrates that the probability of crack propagation in a structure may be reduced considerably by judicious selection of constraints on the structure guided by strain energy release rate computations.

References

[1] GRIFFITH, A. A., "The Phenomena of Rupture and Flow in Solids," Phil. Trans. Roy. Soc., London, pp. 163-198, 1920.

[2] CHOPRA, P. S., WANG, P. Y. and HARTZ, B. J., "Probabilistic Prediction of Multiple Fracture under Service Conditions," Nuclear Engineering and Design, Vol. 28, 3, pp. 446-459, 1974.

[3] CHOPRA, P. S., "The Significance of Symmetry in Multiple Fracture Analysis," in Symmetry, Similarity and Group Theoretic Methods in Mechanics, Proc. Symp. University of Calgary, Calgary, Canada, pp. 499-512, August 1974.

[4] WILSON, E. L., "Structural Analysis of Axisymmetric Solids," AIAA J., Vol. 3, 12, December 1965.

[5] TURNER, M. J., CLOUGH, R. W., MARTIN, H. C. and TOPP, J. L., "Stiffness and Deflection Analysis of Complex Structures," J. Aero. Sci., Vol. 23, 9, 1956.

[6] PARIS, P. C. and SIH, G. C., "Stress Analysis of Cracks," in Fracture Toughness Testing and its Applications, ASTM STP 381, pp. 30-81, April 1965.

[7] CHOPRA, P. S., "Finite Element Fracture Mechanics Analysis of Creep Rupture of Fuel Element Cladding," Nuclear Engineering and Design, Vol. 29, 1, pp. 7-21, November 1974.

TABLE I. Strain Energy Stored in the Rectangular Plate for Various Fracture Configurations

	Angle of Crack Propagation			
Condition of Plate	45°	0°	-45°	-90°
Free, Undeformed	3.1448	3.1436	3.1569	3.0971
Free, Deformed	3.1494	3.1479	3.1615	3.1012
Constrained, Undeformed	3.1221	3.1213	3.1307	3.0862
Constrained, Deformed	3.1253	3.1244	3.1339	3.0895

Fig. 1. Photomicrograph of Stress Corrosion Cracking in 2024-T4 Aluminum Alloy

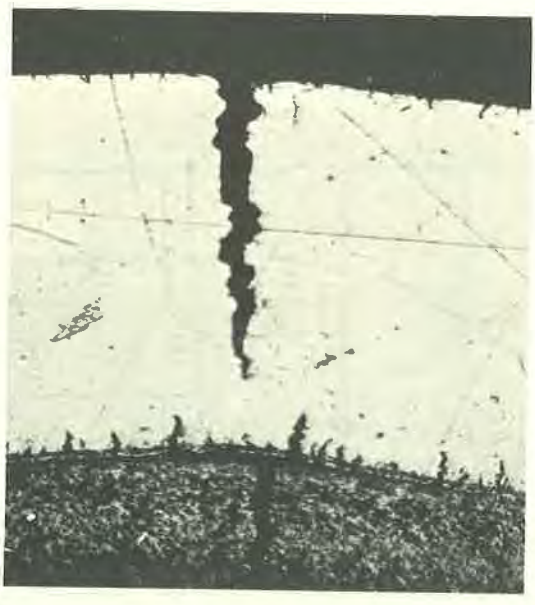

Fig. 2. Multiple and Irregular Fractures in Irradiated Type 304 SS Cladding

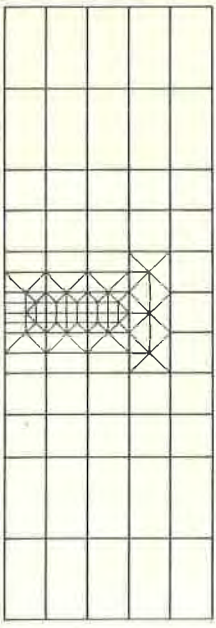

Fig. 3. Finite Element Representation of an Edge-cracked Panel for Investigation of Symmetric and Non-symmetric Multiple Fracture Configurations

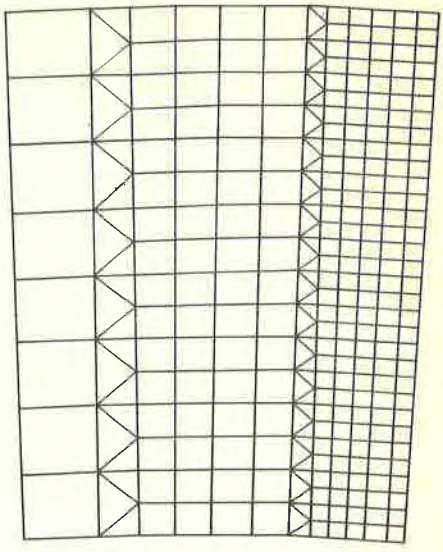

Fig. 4. Finite Element Representation of Part of a Cylindrical Shell Segment

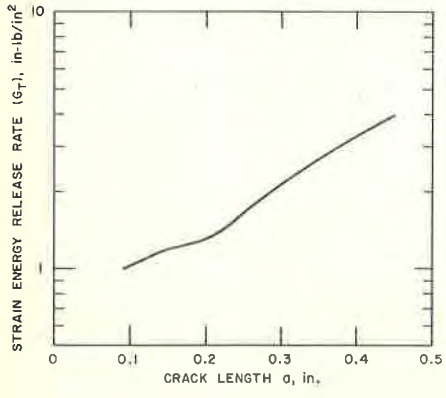

Fig. 5. Results of Finite Element Simulation of Crack Propagation in Rectangular Panel

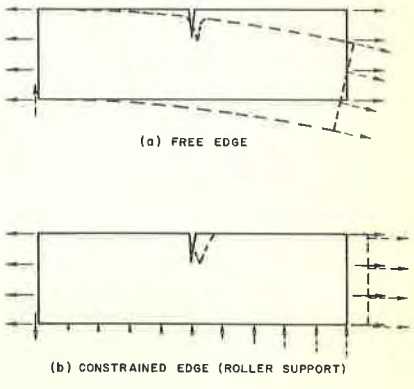

Fig. 6. Free-body Diagram of Undeformed and Deformed Edge-cracked Panel under Uniaxial Tension

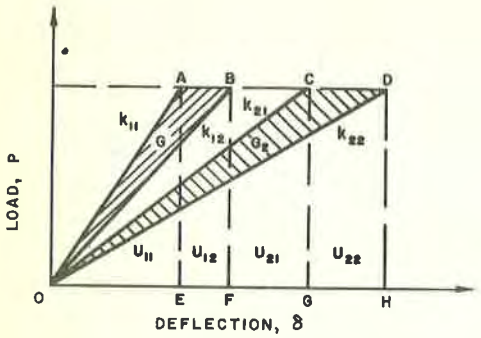

Fig. 7. Schematic Representation of Strain Energy and Total Strain Energy Release Rate

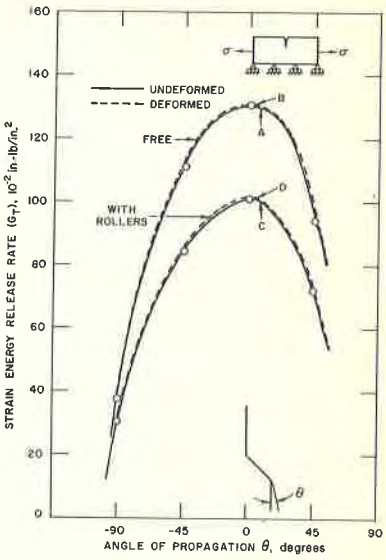

Fig. 8. Total Strain Energy Release Rates for Initially Undeformed and Deformed Edge-cracked Panel

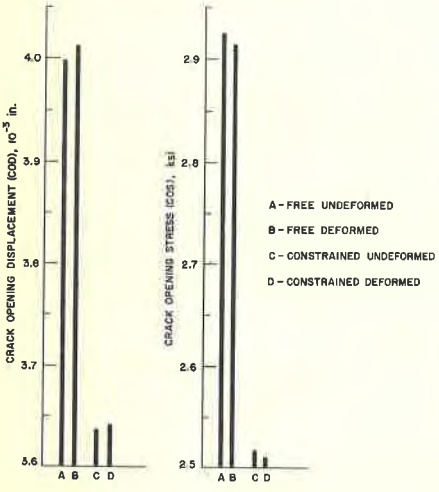

Fig. 9. Crack Opening Displacements and Stresses

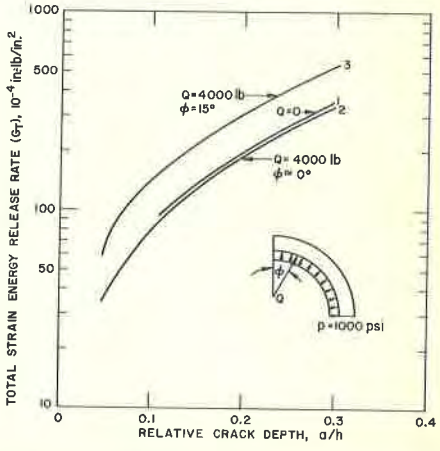

Fig. 10. Total Strain Energy Release Rates for Cylindrical Shell Element

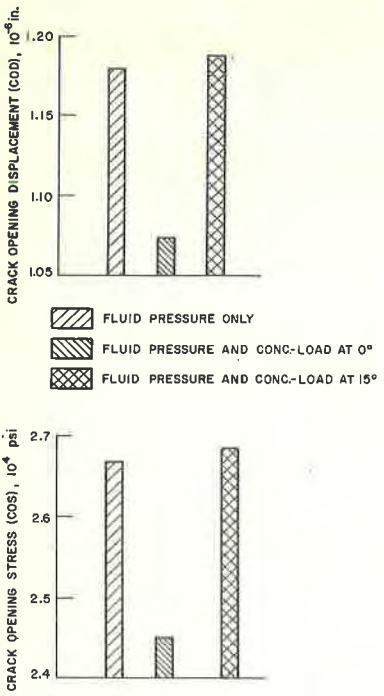

Fig. 11. Crack Opening Displacements and Stresses for Cylindrical Shell Element

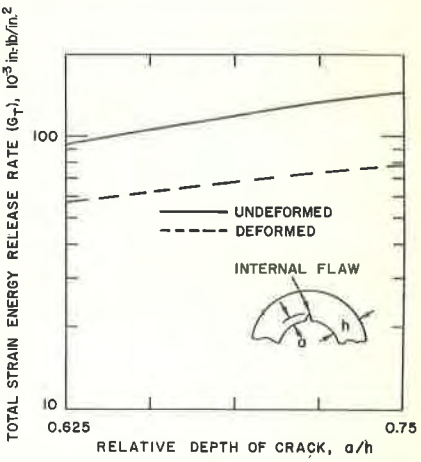

Fig. 12. Total Strain Energy Release Rates for Initially Undeformed and Deforme Cylindrical Shell Element

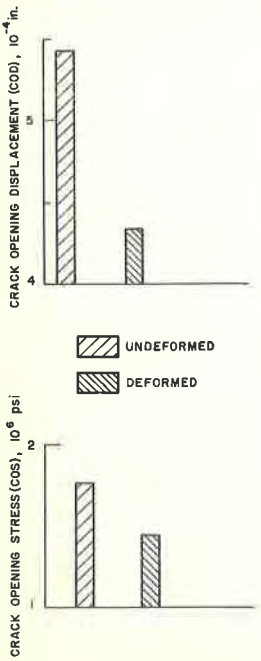

Fig. 13. Crack Opening Displacements and Stresses for Initially Undeformed and Deformed Cylindrical Shell Element

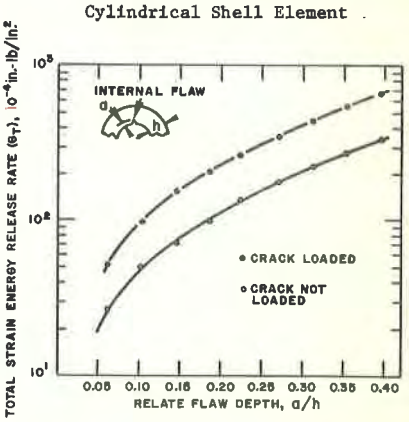

Fig. 14. Total Strain Energy Release Rates for Internal Crack Propagation [7]